https://doi.org/10.15407/ufm.23.03.411

A.V. VOLOKITIN [1,*], I.E. VOLOKITINA [2,], and E.A. PANIN [1]**

[1] Karaganda Industrial University,
Republic Ave., 30, 101400 Temirtau, Kazakhstan
[2] Rudny Industrial Institute,
50 Let Oktyabrya Str., 38, 111500 Rudny, Kazakhstan

* a.volokitin@alservice.kz, ** i.volokitina@alservice.kz

THERMOMECHANICAL TREATMENT OF STAINLESS STEEL PISTON RINGS

We study the influence of thermomechanical processing, namely, severe plastic deformation by high-pressure torsion and cryogenic cooling, on the change of the microstructure and mechanical properties of the piston rings made of AISI-316 stainless steel. The deformation of the annular workpieces is carried out in a tool of a new design, the key feature of which is a double helix system. In the first part of the experiment, an estimation simulation of the high-pressure torsion process is carried out in a new matrix design. To estimate the process possibility, the main technological parameters of the process are varied in order to determine the most optimal conditions. Parameters such as the workpiece heating temperature, the upper striker vertical speed, and the friction coefficient at the contact of the workpiece with the tool are selected. The stress–strain state of the annular workpiece during deformation is also studied. At the second stage of the study, a laboratory experiment on the annular blanks deformation is performed. The microstructure evolution and mechanical properties of deformed workpieces after 8 cycles of deformation by high-pressure torsion at cryogenic temperature are studied. All the metallographic studies are carried out using the modern methods such as transmission electron microscopy and analysis of diffraction patterns of back-reflected electrons. As a deformation result, a nanocrystalline structure with a size of 30–40 microns with a large number of large-angle boundaries and a high complex of mechanical properties is obtained. The tensile strength rises from 595 MPa to 1965 MPa, while the yield strength rises from 320 to 1280 MPa. The plasticity value decreases from 55% to 24% as compared to the initial state, but it remains at a sufficient level to be applied.

Keywords: severe plastic deformation, piston rings, stainless steel, microstructure, mechanical properties, cryogenic cooling.

Citation: A.V. Volokitin, I.E. Volokitina, and E.A. Panin, Thermomechanical Treatment of Stainless Steel Piston Rings, *Progress in Physics of Metals*, **23**, No. 3: 411–437 (2022)

1. Introduction

1.1. The Severe Plastic Deformation Methods as the Potential Ways of Piston Rings Processing

Piston rings are special open-type rings, which have a small gap in their structure and are planted in the piston grooves of the power plant. All the piston rings are distinguished as two main types: oil-removing and compression rings [1].

Compression rings are a type of piston rings of a car engine that prevent the penetration or breakthrough of gases from the combustion chamber of the cylinders into the crankcase of the power plant. As a rule, the outer diameter of such rings in the free state will be smaller than the inner diameter of the cylinder. Note that a small section of compression rings is specially cut off; such a cut out in these details is called a lock. Oil-removing rings are a type of piston rings that prevent the penetration of engine oil from the engine crankcase into the combustion chamber and ensure the removal of excess oil from the cylinder walls. Rings of this type are installed in the power plant below the compression level. The main design difference between oil-removing rings and compression rings is the presence of the first special through holes [2].

Piston rings are the most important antifriction parts of an internal combustion engine, therefore high requirements are imposed on their material, both in terms of physical and mechanical, and a number of special properties.

In modern engines, piston rings are subjected to dynamic loads that affect the fatigue strength of the material. In this case, there is a need to increase their additional strength while maintaining the stability of elastic properties and preventing their breakdowns.

The elastic-properties' stability of piston rings and the prevention of their breakdowns are achieved by choosing the optimal compositions and alloys, manufacturing technology, methods of thermal or thermomechanical processing. Therefore, manufacturers of internal combustion engines around the world are constantly searching for new technologies in the manufacture of piston rings.

One of the main tasks of physical materials science is to provide the required combination of technological and operational properties of modern materials. Mechanical properties depend on such structural parameters as grain sizes, dislocation density, and types of intercrystalline boundaries [3, 4]. The simplest and most effective way to obtain materials with an ultrafine-grained structure is thermomechanical processing (TMP) based on a combination of large plastic deformations and annealing [5, 6]. By varying the TMP modes, it is possible to obtain structures with different parameters as a result of the development of

certain recrystallization processes, which makes it possible to control the properties of materials in a wide range due to microstructural design.

To date, great attention of scientists is paid to the study of methods that allow obtaining ultrafine-grained (UFG) or even nanostructure. It is possible to obtain ultrafine-grained and nanostructured materials in macro volumes in two fundamentally different ways, namely, compacting the mass of already obtained isolated particles of material having the appropriate size or using the severe plastic deformation (SPD) with grinding the size of the structural units to the desired ones.

The first method involves controlled condensation of crystals from the gas phase or grinding the material in ball mills to the state of an ultrafine powder and, then, compacting it into a finished part [7, 8]. This method has a number of disadvantages associated with the residual porosity of finished products, geometric limitations on the dimensions of the parts obtained and the inevitable impurities of impurities in the powder. In addition, the technological and economic part of the issue is very important, which is expressed in the need to use two complex and very energy-intensive processes on complex equipment in sequence.

The severe plastic deformation methods are devoid of described disadvantages. According to numerous studies [9–13], the production of equiaxed UFG grains with high-angle boundaries by this method is possible under the following conditions:

(i) achieving high degrees of strain for grain grinding (>6–8);

(ii) formation of high hydrostatic pressure preventing the destruction of the sample and annihilation of crystal lattice defects (1 GPa and higher);

(iii) deformation at temperatures of 0.4 melting point and below, preventing recrystallization;

(iv) ensuring turbulence and non-monotonicity of deformation, contributing to the formation of high-angle intergrain boundaries.

Similar conditions can be obtained by such methods as high-pressure torsion, equal-channel angular pressing, screw extrusion, multiaxial forging and others.

One of the widely known SPD methods is equal-channel angular pressing (ECAP) [14, 15]. The ECAP method makes it possible to obtain volumetric prismatic samples with a homogeneous UFG structure at a grain size of 100–200 nm and does not require complex equipment. The method consists in pushing the workpiece through the angular channel of the matrix and implements a simple shift scheme. The transverse dimensions of the workpiece remain unchanged during deformation, thereby allowing multiple processing of one sample, which leads to large applied deformations.

The ECAP allows materials to be subjected to large plastic deformations without changing the workpiece cross-section, which makes it possible for them to be redeformed. However, the formation of fine-grained

structures by ECAP depends on many factors, such as the number of passes, the route, the deformation temperature, the angle of channels intersection, the rounding radius at the channels intersection, the pressing speed, the sample material, lubricant that reduces the friction coefficient between channels and material. This method is the most studied and is one of the most frequently mentioned in scientific articles devoted to the study of various UFG materials.

Over the past two decades, the work related to equal-channel angular pressing of metal materials has aroused considerable interest among researchers in the field of materials science and metal physics. One of the main objectives of the work was to grind the grains of metals and alloys of various compositions to a fine-grained or ultrafine-grained state (grain size less than 10 or 1 microns, respectively), which ensured the achievement of a unique set of mechanical and physical properties. Another purpose of the research was to study the basic laws and mechanisms of the formation of ultrafine-grained microstructure in the severe plastic deformations processes, since equal-channel angular pressing can ideally achieve arbitrarily large deformation degrees, without changing the shape and size of the pressed blanks [16]. In addition, this method has many variations of technical and technological execution presented in patents of different countries.

The improvements are mainly aimed at increasing the degree of deformation in one pass, and increasing the uniformity of the study of the structure throughout the volume. The most attention will be paid to the stepped ECA matrix (ECA matrix with parallel channels in some sources) [17, 18], which allows to realize two alternating deformation zones at once, provided that the input and output channels are co-directional. This scheme is also energy saving, since it allows you to realize a large deformation degree in one pass with the same effort. Due to the directionality of the input and output channels and a relatively small pressing force, matrices of this type are most convenient for creating combined processes.

A variant of ECAP with an angle less than 90° has also been developed. For example, in work [19], the ECAP method in matrix with a 45°-channel junction angle and a special form of channel coupling was proposed, providing the highest deformation degree per pass, with reduced force and maintaining the correct shape of the front end of the workpiece.

In the method described in Ref. [20], combined severe plastic deformation is carried out in the following sequence: torsion deformation in a screw channel, then the workpiece passes into a section of the matrix that implements equal-channel angular pressing. When pressing the workpiece through the screw channel of the matrix, it obtains severe shear deformation mainly in cross-section, which is superimposed with a homogeneous intense volumetric shear deformation during subsequent

pressing. During the full pressing cycle, the structure is crushed in the material of the workpieces, while the proposed sequence leads to a more isotropic structural state. This is explained by the fact that a less homogeneous torsion deformation is superimposed by a more homogeneous and intense shear deformation during compression, which smooths out the resulting inhomogeneity after torsion, both structurally and in obtaining more homogeneous properties. The reverse sequence leads to the imposition of a more heterogeneous state on a homogeneous one, which is fixed in the workpiece after pressing, while all the known methods of the pressure treatment show that the values of these characteristics of the material in different directions of the workpiece differ significantly.

There is also a tendency to create multi-angle equal-channel matrices (equal channels multi angular extrusion, ECMAE) in order to implement alternating deformations. The most interesting solutions are presented in works [21–24]. These methods increase the degree and uniformity of deformation in one pass, but require significantly more effort and are not suitable for all the materials and temperature–velocity deformation conditions.

Pressing in those tools is accompanied by a change in the shear direction in the next zone, including the opposite. In each zone, the main deformation axes undergo rotation, and when the material passes through each subsequent zone, the axes rotation direction changes to the opposite. This contributes to the effective fragmentation of structural components and the formation of structure isotropy in each deformation cycle. With each subsequent zone and deformation cycle, because of the appearance of a large number of directions, in which an elementary shift in the microvolumes of the deformable material can occur, the microdistortions of the crystal lattice are redistributed between individual microvolumes of the plastically deformable material. This also contributes to the intensive process of crushing mosaic blocks and individual crystallites, because of which a finely dispersed structure is observed [25].

With these methods, the hardening intensity is less than with traditional monotonous plastic deformation (*e.g.*, hydroextrusion) due to some relaxation of microstresses because of more intensive structure crushing with intermittent alternating course of the deformation process.

With all the described advantages of multiangle ECAP in the formation of a homogeneous UFG and nanostructure, it also has disadvantages associated with a large effort or with the need for a large number of passes, or is not suitable for all the materials and temperature–velocity deformation conditions.

The described methods and devices are the most effective and popular for obtaining UFG and nanostructures. However, there are other methods, which also allow obtaining UFG products by severe plastic deformation.

The screw extrusion method (SE) proposed in Ref. [26] differs from the known methods by the stress-strain state in the sample, as well as technological possibilities of application. SE allows accumulating large deformations in metals, noticeably grinding their microstructure and can be implemented in hydroextrusion plants to produce precision long-length profiles of different shapes (rods, pipes, drills, *etc.*). However, it can lead to the appearance of strong undesirable anisotropy, for example, in pure titanium. The use of subsequent rolling makes it possible to reduce significantly the degree of anisotropy caused by SE [27].

The SE essence is that the prismatic blank is pressed through a screw matrix, the channel of which consists of three sections: entrance, screw and calibration. The geometric parameters of the cross-sections of all the sections are the same. The characteristic of the helical section is the inclination angle of the helical line furthest from the matrix axis to the extrusion axis.

Due to the specified features of the channel geometry, when the workpiece is pushed through it, its shape does not change, which allows multiple extrusion in order to accumulate severe deformations. At the same time, its structure and properties change while maintaining the identity of the initial and final forms. The geometric parameters of all the cross-sections are the same. The fibre located along the axis of the sample undergoes minimal deformation; the fibres furthest from the axis undergo maximum deformation [28, 29].

Comprehensive forging (multiaxial forging, 3*D* forging) [30] can also be used to form UFG and nanostructures in massive samples. The process of comprehensive forging is usually accompanied by dynamic recrystallization. Closed forging is a modification of the comprehensive forging process [31]. Comprehensive isothermal forging is a type of deformation processing that allows obtaining an ultrafine-grained structure in massive workpieces without changing the original geometry.

The main idea is a series of sediments by 40–60% in a closed die with a change of the deformation axis by 90° [32], which make it possible to work out 'stagnant' deformation zones [33]. Hydraulic and mechanical presses, as well as hammers, are used as deforming equipment for forging. For the first two types of presses, the strain rates vary in the range of 10^{-2}–10 s^{-1}, in the case of a hammer from 10^2 s^{-1} and higher [34]. It is known that, for greater workability of the structure, it is advisable to use low speeds, which increase the deformation ability, as well as reduce heating during deformation. In addition, the use of closed and semi-closed stamps is appropriate for this purpose: greater uniformity of deformation and stable geometry is achieved.

The scheme of comprehensive forging is based on the use of multiple repetitions of free forging operations: draft-broach with an axis change of the applied deforming force. The deformation uniformity in this

technological scheme in comparison with ECAP or torsion is lower. However, this method makes it possible to obtain an UFG state in sufficiently fragile materials, since processing begins with elevated temperatures and small specific loads on the tool are provided. The choice of appropriate temperature-velocity deformation conditions makes it possible to obtain very fine grains of about 100–500 nm in pure metals and less than 100 nm in alloys. This approach is usually implemented at plastic deformation temperatures in the range (0.3–0.6) of the melting point. Disadvantages of forging processes are their high labour and energy intensity, with an inhomogeneous strain distribution over the workpiece volume.

High-pressure torsion (HPT), as the Bridgman anvil evolution, was one of the first methods for obtaining volumetric UFG and nanostructured samples, later developed in [34–36]. This method was developed by P.W. Bridgman (Nobel Prize in Physics in 1946) and further developed in the works of L.F. Vereshchagin, N.S. Enikolopyan, V.E. Panin and other scientists from USA, Austria, Japan, China, and RF. Samples in the disk form with a diameter of 10–20 mm and a thickness of 0.3–1 mm are deformed by torsion under conditions of high applied hydrostatic pressure. The sample is placed inside the cavity made in the lower striker, and a hydrostatic pressure of 1 to 10 GPa is applied to it. Plastic deformation by torsion is carried out due to rotation of one of the strikers. Turning the movable anvil at a certain angle allows achieving varying deformation degrees. The use of hydrostatic pressure makes it possible to prevent the sample destruction during deformation, while it is possible to achieve large deformation degrees.

The sample geometric shape is such that the material bulk is deformed under quasi-hydrostatic compression under the action of applied pressure and pressure from the sample outer layers. As a result, the deformable sample despite a large deformation degree is not destructed. At the same time, the sample deformation has a radial inhomogeneity, which, according to studies [34–37], can be minimized by a large number of revolutions. The high-pressure torsion method is also possible to process the workpiece in the ring form, according to the scheme proposed by S. Erbel [38]. This method has improvements aimed at increasing the structure uniformity in the centre and on the periphery of the sample, manufacturability and expansion of the types of materials produced.

Thus, in work [39] it is proposed to carry out a cyclic change in the specific pressure by 10–20% of the current value with a frequency of 0.1–1.5 of the set rotation speed of the striker during HPT. In addition, the task is achieved by changing the direction of rotation of the striker with a step of 0.1–1.5 turns during deformation.

The technical result is achieved by the fact that the load cycling during HPT leads to a change in the material vacancies' concentration,

which affects the dislocation crawling rate and on the mechanisms of deformation and ultrafine-grained structure formation, ensuring its uniformity. The load cycling at HPT is similar to the sample rotation during ECAP, which leads to a change of sliding systems during processing and thereby provides a more uniform microstructure of the material and an increase in physical and mechanical properties, such as tensile strength and microhardness. It was established that SPD by HPT method affects the material structure, increases the density of crystal lattice defects; the material processed by HPT is deformed inhomogeneously along the radius, as a result the grains removed from the centre are deformed more, which leads to their fragmentation. As a result, the material structure becomes fine-grained and it affects the mechanical and functional properties of the material, such as strength, ductility, electrical conductivity, *etc*. Using HPT method, many researchers in many materials managed to obtain a structure with the smallest grain size (up to 20 nm), study its features and evaluate a number of their mechanical and physical properties.

Hydrostatic extrusion (HE) is successfully used to induce severe plastic deformations in bulk metals and to produce UFG and nanostructures [40]. Hydrostatic extrusion carried out at ambient temperature makes it possible to grind the structure more strongly than conventional plastic deformation methods (for example, rolling, extrusion, drawing, forging, ECAP, *etc*.). In normal deformation processes, the deformation per pass cannot be large, since deformation hardening can lead to cracking of the material.

During hydrostatic extrusion, due to ultra-high all-round pressure, the structure microdefects of the extruded material close and its plasticity increases sharply. Due to this, it becomes possible to obtain profiles of complex shape from fine plastic and brittle materials that could not be processed by extrusion with a rigid punch. In addition, due to deformation under conditions of high all-round pressure, the structure of processed metals and alloys improves.

Based on the analysis of the methods described above for obtaining an ultrafine-grained structure, high-pressure torsion is the most suitable method for piston rings processing and improving their operational properties.

1.2. Materials for the Piston Rings Manufacture

The materials for the piston rings manufacture have to be selected taking into account the antifriction properties and the conditions under which the piston rings should work. High elasticity and corrosion resistance are important as well as high resistance to damage under extreme operating conditions.

Most piston rings are made of a cast iron as a common material in the automotive industry. The structure of this material allows the rings to hold the engine oil, thereby reducing the wear of the power plant. The most popular type of cast iron in the piston rings production is ductile iron. This type of cast iron has many positive qualities, the most important of which is the ability to deform elastically. This quality facilitates the process of installing rings in the grooves of pistons [2].

In addition to the material described above, there is another one, which was created in order to increase the rings service life, as well as to ensure their accelerated running-in. The basis of such material is cast iron, and the outer surface consists of a molybdenum coating. Unlike chromium, molybdenum has anti-wear properties and has greater resistance to mechanical influences. To date, most modern engines are assembled with molybdenum piston rings, as they are more reliable, durable than steel and cast iron, and are easily adjusted to the power plant nodes.

The next type of material from which piston rings are made is stainless steel. This material is an improved type of chrome-plated cast iron. Stainless steel is a material that contains a certain amount of chromium. Such rings almost do not differ in properties from chrome ones. Unlike rings made of cast iron, steel elements are better able to withstand high temperature, as well as its sharp drop. To increase wear resistance, the surface of such steels is subjected to hardening. This is usually done by nitriding. In addition, coatings that improve rheological properties are applied to the piston rings surface. At the same time, priority is given to increasing wear resistance, as well as ensuring compaction in extreme conditions.

However, the nitriding process takes a very long time, and when applying the coating, the layers deposited on the working surfaces often peel off. The reason for this is mainly errors in the piston rings installation (too much stretching when installed on the piston or rings deformation). In addition, in the structure of hardened stainless steel, there is a certain amount of fairly soft residual austenite, which is due to its chemical composition and heat treatment mode. As a result, hardness, strength, thermal conductivity and magnetic properties decrease, the steel viscosity increases, the dimensions change, and the surface quality of the product deteriorates. Tempering of hardened steel in order to eliminate or reduce the amount of residual austenite is ineffective in most cases, since the necessary degree of decomposition of residual austenite and its replacement with martensite is not achieved. To improve the structure of hardened steel, reduce the amount of austenite in its composition, improve the quality and strength of products, it is most rational to use the cryogenic method of metal processing (processing and exposure to cold, deep cooling).

Recent years, the demand for austenitic stainless steel has increased significantly. This material is often chosen because of its high corrosion resistance and good formability. However, most austenitic steels suffer from low yield strength, which limits their technological application. The task is to strengthen these materials without compromising their useful properties.

1.3. The Cryogenic Cooling Effect during the SPD

In recent years, there has been an increased interest in using the deformation possibilities at the liquid nitrogen temperature or near [41–47]. Such processing is not accompanied by dynamic return or recrystallization, which makes it possible to grind the grain structure more efficiently. Cryogenic treatment provides improved mechanical properties, increased wear resistance and hardness. The surfaces quality subjected to polishing or finishing is improved (the presence of soft and viscous austenitic areas in the structure of the surface layer prevents the creation of a homogeneous mirror surface), which is necessary for piston rings.

Cryogenic cooling is also used in the production of nanostructured metals, using various types of severe plastic deformation. Deep deformation of metals (up to 80–90%) is combined with heat treatment at the liquid nitrogen temperature.

As described above, the SPD methods, in contrast to traditional methods of metal forming, aimed primarily at shaping, are used to significantly change the structure, phase composition, physical and mechanical properties. As a result, the length of grain and subgrain boundaries increases by orders, the static and dynamic dilation of the atoms of the crystal lattice changes markedly. Due to this, the strength characteristics of metals increase many times while maintaining sufficiently high plastic properties [48–53].

The high hydrostatic pressure associated with hydrostatic extrusion, which increases the metal ductility, plays a very useful role in cryoprocessing, in which solids become more brittle compared to those that undergo deformation at ambient temperature. On the other hand, the triaxial compressive stress state induced by hydrostatic extrusion preserves the material adhesion even with much larger contractions per pass. It is expected that the high hydrostatic pressure applied during deformation will prevent the unfavourable increase in brittleness characteristic of metals at low temperatures. Therefore, the authors [40] propose a hydrostatic extrusion conducted at cryogenic temperature, which gives a more favourable compromise between the strength and ductility. This was achieved due to the increased dislocations mobility and their increased density.

As described above, a good combination of strength and plasticity is obtained using ECAP. Such high strength and hardness is obtained by reducing the grain size to an ultrafine-grained state, deformation hardening also occurs due to dislocation hardening and an increase in the proportion of high-angle grain boundaries. At ambient temperature, deformed workpieces demonstrate increased mechanical strength due to an increase in the pass number along with very small-elongated grains reaching nanoscale. Cryogenic deformation by ECAP method was carried out for pure titanium, a decrease in the temperature of ECAP and an increase in the pass number led to the microstructure change with a smaller average grain size. Deformation of copper up to 16 passes and aging at 700 °C slightly increase the hardness and yield strength of the deformable material, but aging at 100 °C relatively improves these properties due to residual hardening, although it does not affect plasticity. Samples after ECAP can be processed by cold rolling or cryorolling. Cryoprocessing at low temperature strengthens the material by reducing the grain size and increasing the dislocation density, which leads to immobilization or difficulty in the dislocations movement [54, 55].

In addition, due to the dislocation short movement free path, the UFG microstructure has a weak interaction with dislocations, which leads to low hardening, plastic instability and early neck formation during stretching, leading to limited plastic deformation [56].

High strength with high ductility can be realized in metals and alloys using bimodal grain size distribution, where large grains provide ductility and small grains carry the main load to provide most of the strength. In Ref. [57], a bimodal grain size distribution with high strength and ductility in Cu was reported using ECAP followed by cryoprocessing and instant annealing for a short time. Annealing for a short time after deformation causes abnormal grain growth in a limited number of grains.

One of the HPT disadvantages is the extreme grain grinding, especially in pure metals, in the range of 300–500 nm. The limitation of grain grinding with an increase in the deformation degree by traditional SPD methods is explained by the release of heat during deformation, which does not have time to be removed. As a result, the sample temperature increases noticeably. The formation of a recrystallized structure in the alloy indicates that the sample is heated to dynamic recrystallization temperatures during the HPT process.

The work [58] describes a method for obtaining products from magnetically soft amorphous alloys by HPT with cryogenic deformation temperature. This approach makes it possible to improve the magnetic (hysteresis) characteristics of amorphous soft magnetic alloys by grinding the structural units of the material to 100 nm or less. Here, for ultra-high grinding, the authors ensured the lowest possible tempera-

tures, despite the fact that deformation of such materials without destruction, especially at low temperatures, is possible only under high hydrostatic pressure.

Another advantage of obtaining an ultrafine grain microstructure by cryoprocessing over methods of severe plastic deformation is due to the difference in the process of grain fragmentation and the nature of grain boundaries. In cryorolling, grain fragmentation is facilitated by suppressing dynamic recovery at cryogenic temperature, and the simultaneous occurrence of dynamic recovery and recrystallization promotes grain grinding by SPD methods [59].

In particular, it was shown in [60, 61] that the microstructure of the initial coarse-grained copper and aluminium after cryogenic deformation is characterized by significantly smaller grain sizes than after conventional cold deformation. In this regard, it is of interest to use intensive cooling in liquid nitrogen during deformation, which will allow obtaining a close to optimal combination of strength and ductility of the material.

Therefore, it is proposed to manufacture rings from stainless steel blanks with high mechanical strength, due to optimal thermomechanical deformation hardening during the high-pressure torsion and cryogenic cooling. Stainless steel is corrosion-resistant and when creating certain structural and mechanical states with the help of the proposed thermomechanical treatment and increasing its operational properties, the service life of piston rings will increase.

2. Materials and Methods

2.1. Simulation of Process

At the previous stage of work [62, 63], a new design tool was developed to implement the high-pressure torsion process of annular workpieces. It was found that, for successful implementation, it is necessary to ensure the torsion of the deforming tool with the constant rectilinear movement of the upper striker of the press. The solution of this technical problem can be implemented in practice only in the presence of a composite deforming tool that includes both displacement and rotation blocks. In this system, periodic spiral grooves of the same shapes and sizes are created on two contacting surfaces. With mutual movement towards each other and rotation of at least one body around its axis, the contours of the spiral cut-outs begin to mate up to full contact. In our case, the rotational motion will be communicated to the idle element due to sliding friction between two spiral surfaces (Fig. 1).

Figure 1, *a* shows a three-dimensional model of the upper striker, which is obtained the forward movement from the press. The 4 periodic recesses of spiral shape have been created on the lower face. At the same

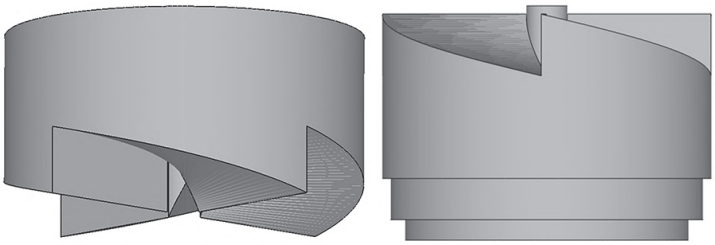

a *b*

Fig. 1. Tool design: upper striker model (*a*) and lower striker model (*b*) [63]

time, a cylindrical hole is provided in the centre of the striker for the rod of the deforming element and ensuring the alignment of both strikers. Figure 1, *b* shows a three-dimensional model of the lower striker, which is informed by the torque from the translational motion of the upper striker. Due to sliding friction between two spiral surfaces, this element is forced to rotate around its axis until the vertical sections of the spiral channels close.

In order to assess the possibility of a process stable flow, a simulation by the finite element method in the Deform program was carried out. The initial blank had an annular shape with a diameter of 76 mm, a width of 3.5 mm and a thickness of 3 mm. AISI-316 austenitic stainless steel as the material of the workpiece was chosen. The deformation at ambient and cryogenic temperatures was carried out. A non-isothermal type of calculation was established. An absolute tetrahedral grid on the blank was built. The minimum size of the element was set to 0.3 mm, the maximum size of the element was set to 0.6 mm, and the parameters of the grid remeshing were set by default.

The movement speed of the upper striker was of 1.5 mm/s. To carry out shear deformation in this process, a high degree of adhesion of the workpiece with the tool is necessary. Therefore, at the contact of the workpiece with the lower striker and the deforming element, the value of the friction coefficient was set to 0.45. No velocity values were reported to the deforming element. Instead, the following boundary condition was set on the axis of the cylindrical rod: free movement in the vertical direction; axis movement in the other two directions was disabled. This fixation corresponds to the fact that the rod falls into the cylindrical hollow of the upper striker and can freely move and rotate in it.

In addition, rotation around this axis was allowed for all the spiral surfaces of the deforming element. At the same time, the value of the rotation angular velocity was also not set, instead, an extremely small torque value of 10^{-6} N·mm was set with a sign opposite to the rotation intended direction. This method is universal when it is required to set

an indirect rotation from the action of friction forces. At the contact of two spiral surfaces, a small friction coefficient value equal to 0.1 was established, which in real conditions is provided by a low level of roughness of both surfaces and the use of lubrication.

The simplest way to assess the real possibility of implementing any process is to consider the resulting deformation force, since this parameter determines the real deformation capabilities of the mechanical equipment used. The resulting deformation force on the first two cycles was considered. About 464 kN was obtained in the first cycle, and circa 1200 kN was obtained in the second cycle. These values are quite adequate, given the complex loading scheme and the sufficiently durable source material.

At the next stage, it was decided to vary the main technological parameters of the process in order to determine the most optimal conditions for the high-pressure torsion process implementation. When choosing variable parameters during simulation, it is advisable to use those parameters that are easy enough to change in real conditions. The following parameters were selected: workpiece heating temperature (easily changed by heating in a furnace or cooling in liquid nitrogen), vertical speed of upper striker (easily changed by press control panel) and friction coefficient at the contact of the workpiece with the tool (easily changed by using technological lubrication).

After determining the list of variable parameters, it is necessary to select their values for variation. For the workpiece temperature, it is advisable to choose the same values in both directions from the set ambient temperature in order to assess the effect of heating or cooling. When cooled in liquid nitrogen, the metal cools to a temperature of –196 °C. Therefore, the values of –196 °C and +196 °C were chosen.

To simulate the material mechanical properties at cryogenic conditions, it is necessary to include the appropriate information in the Deform program. All the necessary parameters were determined according to the data given in work [64], where data for temperature –200 °C were described. As a result, a new hardening curve for the Deform program at a temperature of –200 °C was obtained.

The upper striker vertical speed was set quite small by default (1.5 mm/s); so, a higher value of 15 mm/s was chosen [18]. It will be irrational to use the lower values of the upper striker speed, since, in this case, the process duration will be excessively long, which will lead to annihilation of the workpiece temperature effect, regardless of the temperature value (positive or negative), with prolonged contact of the workpiece with the tool, the workpiece temperature will align with the tool temperature.

The friction coefficient at the contact of the workpiece with the tool was set high enough by default (0.45) to ensure an adhesion high level

of the workpiece with the tool. Increasing this value will be quite problematic, since the tool will have to be machined. At the same time, it is quite easy to reduce the value of the friction coefficient by using technological lubrication. The value of the friction coefficient of 0.15 was used. This value is the recommended for cold deformation processes with prolonged contact of the workpiece and the tool.

2.2. Laboratory Experiment

The experimental HPT equipment was made of 5KHV2S steel on a CNC turning and milling machine. The structural components after manufacture were subjected to special heat treatment to increase the strength properties. After manufacturing all the structural elements, it was assembled. Thus, the lower holder was installed on the base of the hydraulic press plate and secured with tie bolts through the retaining corners (Fig. 2). A lower striker is installed in the lower holder, with a chamber for ring deformation; the upper striker is installed on top of the sample.

The experiment itself was carried out in the laboratory on a single-column hot-stamping crank press of PB 6330-02 model. The number of deformation cycles was 8. The deformation temperature was –196 °C.

To obtain a single-phase γ-structure, a standard heat treatment was applied, which includes heating to a temperature of 1100 °C, holding for 30 minutes and cooling in water. As a result of such heat treatment, a γ-solid solution with a homogeneous distribution of alloying elements is fixed in chromium–nickel corrosion-resistant steels, in which there are no carbide secretions, which provides the best corrosion properties. The resulting structure and properties were taken as the original ones.

Metallographic analysis in transverse and longitudinal sections was carried out using an electron transmission microscope JEM 2100.

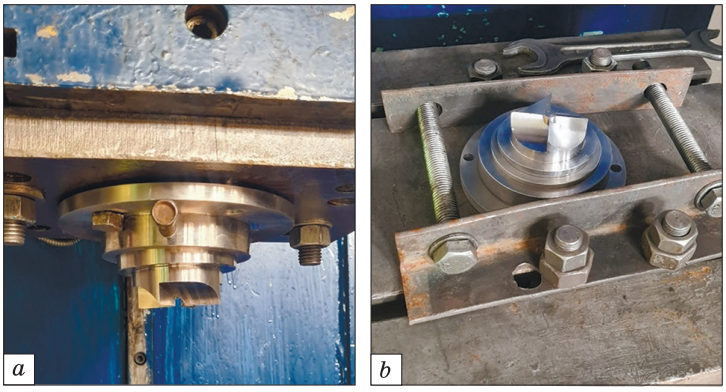

Fig. 2. Assembly of the structure: the upper holder with the upper striker installed in it (*a*) and the lower holder with the matrix installed (*b*)

All the samples were tested in the middle plane to avoid the influence of peripheral areas. The samples preparation for metallographic analysis was carried out at the Struers electrolytic sample preparation facility.

Mechanical tests for uniaxial tension were carried out at ambient temperature on an Instron 5882 machine with a strain rate of 1.0 mm/min. The deformation of the sample was measured by an Instron strain gauge. Tensile tests were carried out on flat samples cut out of the ring (the dimensions of the working part are $3.0 \times 3.0 \times 6.0$ mm) in accordance with the recommendations of GOST (state standard) 1497-84. According to the results of tensile tests of mechanical properties, the characteristics of strength and plasticity were determined: yield strength, tensile strength, and maximum elongation to failure. Microhardness according to the Vickers method was determined using an automatic microhardness meter DM-8 (Affri).

3. Results and Discussion

3.1. Simulation Results

The variation of the main technological parameters in order to determine the most optimal conditions for the high-pressure torsion implementation showed that in all the models at both deformation stages sufficiently adequate force values arise. At the same time, as noted, an increase in the workpiece temperature significantly reduces the deformation force, which is a consequence of a decrease in the deformation resistance level. A decrease in the friction coefficient also significantly reduces the deformation force, which is a consequence of a decrease in the adhesive level at the workpiece-tool contact. The change in the punch speed has a negligible effect on the amount of force. In particular, with an increase in the strain rate, the deformation heating level of the metal increases. As a result, due to a more intense increase in temperature, the deformation force is reduced. The only model, in which an increase in the magnitude of the force was recorded, is a model with a reduced temperature of the workpiece to –196 °C. Here, at the first stage, the deformation force increased by 48%, and at the second stage, it increased by 33%. The decrease in the level of force growth is associated with the gradual deformation heating of the cooled metal.

However, despite the fact that quite adequate force values were obtained in all the models, not all of the considered process conditions are optimal. In particular, a model with a reduced friction coefficient to 0.15 can be considered as unsuccessful, since, at this value of the friction coefficient, the slip of the workpiece was recorded. A model with an increased workpiece temperature up to 196 °C cannot also be called optimal, since, in this case, preheating and subsequent deformation un-

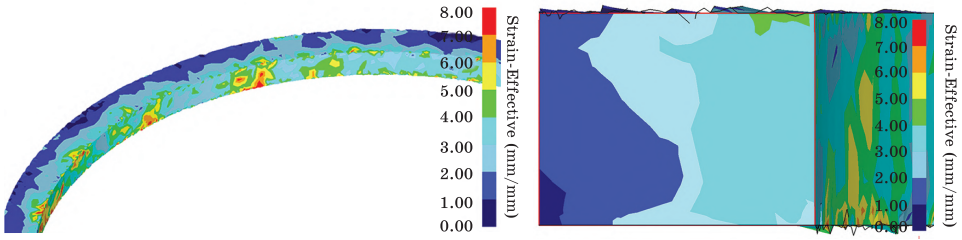

a *b*

Fig. 3. Equivalent strain [66]

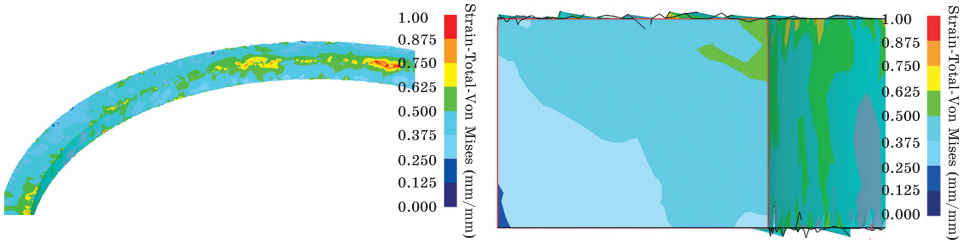

a *b*

Fig. 4. Mises strain [66]

der high pressure cause a significant level of heating of the metal up to 670 °C (unlike the basic model, where heating reaches 360 °C).

The model with an increased punch speed of 15 mm/s practically does not differ from the basic one in its resulting characteristics. The difference is a slight increase in the heating level, which leads to a slight decrease in effort. However, for the practical implementation of these conditions, new pressing equipment operating at increased speeds may be needed. Therefore, it was decided not to consider this model in the future. As a result, a model was chosen to study the stress–strain state at –196 °C (cryogenic cooling).

Figures 3 and 4 show the results of modelling the strain state after the second deformation cycle. The following components were selected as parameters for assessing the processing level: equivalent strain (for analysing the overall processing level) and Mises strain (for assessing the level of shear strain). Additional diametrical incisions were also made to evaluate all the parameters in the cross-section of the annular workpiece. It is established that, at the general level of equivalent strain $\varepsilon \approx 4$, the value of Mises shear strain is approximately $\varepsilon_{Mis} \approx 0.5–0.6$.

It is also necessary to note the differences in the distribution of these parameters. The equivalent strain accumulates mainly on the inner vertical surface of the ring, as well as on the upper face (*i.e.*, on the immediate areas of contact with the moving tool). At the same time, despite the presence of contact of the workpiece with the glass, the de-

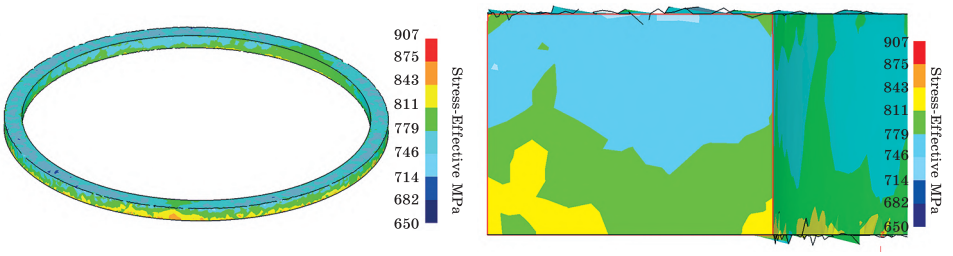

a *b*

Fig. 5. Equivalent stress [66]

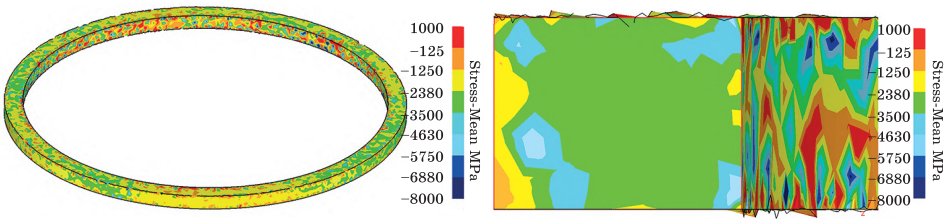

a *b*

Fig. 6. Average hydrostatic pressure [66]

velopment of equivalent strain on the corresponding faces is significantly lower due to the lack of torque in these zones. When analysing Mises strain, the proportion of compressive strain is not considered. Therefore, the level of shear strain development depends more on torsion than on compression. As a result, a characteristic diagonal development of this parameter is observed in the cross-section of the ring, with maximum values in the areas of contact with the moving tool.

Figures 5 and 6 show the results of modelling the stress state after the second deformation cycle. The following components were selected as the evaluation parameters: equivalent stress (to analyse the overall level of developed stresses) and average hydrostatic pressure (to assess the level of tensile and compressive stresses). The level of equivalent stresses shows the average value of the resulting stresses of all the loading schemes, whether it is stretching, compression, torsion, or shear. Considering the section of the workpiece in Fig. 5, it can be noted that the growth of equivalent stresses occurs mainly in the high-altitude (vertical) direction. This suggests that the main part of the strain the workpiece receives from the action of a vertically directed force than from the torque. This fact is also confirmed by the distribution of the parameters of the deformed state, where the proportion of shear strain is about 15%, the remaining proportion of deformations develops from compression. Considering the distribution of equivalent stresses across

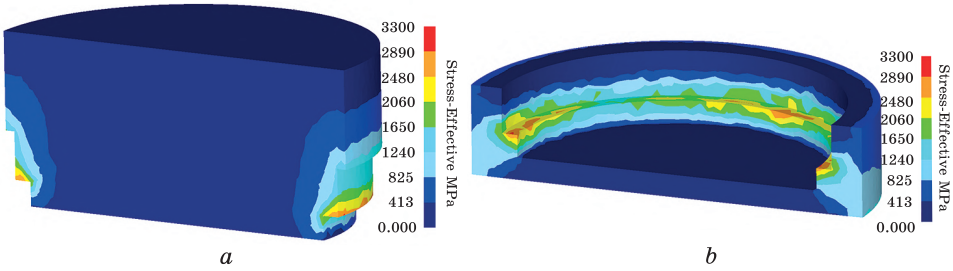

Fig. 7. Stress on the stamp components [66]

the cross-section, it was found that, in the areas of contact with a moving tool (the upper half of the cross-section), the stress values reach 750–770 MPa. In the areas of contact with a stationary glass (the lower half of the section), the stress values reach 810–830 MPa.

The average hydrostatic pressure, in contrast to equivalent stresses, shows the value of the stresses that occur, taking into account the sign, whether it is tension or compression. Therefore, this parameter is the most optimal for studying this loading scheme. Considering the distribution of this parameter in Fig. 6, it can be noted that high compressive stresses occur in the entire cross-section of the workpiece, reaching values of –4500 MPa. At the same time, the level of compressive stresses decreases in the surface layers of all the four faces. In areas of contact with a moving tool, thin zones (less than 0.1 mm thick) of tensile stresses of about 80–100 MPa occur on the surface of the workpiece due to simultaneous compression and torsion.

It was also decided to analyse the stresses arising on the stamp components directly in contact with the workpiece (deforming element and lower striker). These components experience maximum stress during deformation; therefore, at the design stage of experimental tooling, it is necessary to know the stress level experienced by these parts and their dislocations.

Figure 7 shows the results of the stress distribution on these instruments, for the possibility of analysing the stress distribution over the cross-section, diametrical sections are shown. The greatest stress values in both parts occur in the areas of contact with the workpiece; here, the stress values reach 2700–2800 MPa. At the same time, the stress distribution pattern suggests that in both parts, the most dangerous zones in terms of possible wear and cracks are the zones of the steps. As a result, at the stage of tooling creation, it is necessary to provide measures to increase the strength characteristics in these areas.

The simulation showed good results; the next step is a laboratory experiment.

3.2. Experiment Results

The microstructure analysis presented in Fig. 8, *a* showed that the microstructure before deformation is coarse-grained, with an average grain size of 30 microns. The structure of AISI-316 metastable austenitic steel contains ≈100% austenite, polyhedral grains with thin boundaries and annealing doubles. After the 1st pass, the deformation twins begin to appear in a small amount in austenite. After two passes, there is an increase in the number of dislocations near the grain boundaries and the process of martensitic transformation $\gamma \rightarrow \alpha$ begins. Three deformation passes leads to an increase in the austenite structure of a large number of clusters of dislocations adjacent to the deformation twins, which suggest the emergence of a mixed deformation mechanism, including deformation twinning and sliding dislocations at HPT. After the five passes, the grain size decreases to 0.3 microns, shear bands appear in austenite, and the boundaries of the twins become less clearly defined. Eight cycles of deformation at ambient temperature lead to the formation of an equiaxial homogeneous microstructure of 30–40 nm in size (Fig. 8, *b*) with a predominant martensite structure. The formation of the nanostructured state occurs due to the action of two mechanisms. The first mechanism is associated with the fragmentation of the initial grains due to the formation of shear deformation bands and twins of deformation origin, and the second mechanism is associated with the development of the phase transformation $\gamma \rightarrow \alpha$ by the shear mechanism of the formation of deformation martensite. The results of the reduction processes are observed in the structure, since the grains are equiaxed with clearly visible boundaries.

In addition to the microstructure study, the mechanical properties of rings under tension were investigated. As mechanical tensile tests have shown, the nanocrystalline structure of AISI-316 steel obtained in the HPT process has a high complex of mechanical properties. Thus, the tensile strength increased from 595 to 1965 MPa, the yield strength from 320 to 1280 MPa. The plasticity value decreases from 55% to 24% as compared to the initial state, but remains at a sufficient level for use.

The results of the microhardness determination correlate with the data of mechanical tests and indicate that HPT in the new die makes it possible to obtain a sufficiently uniform hardness over the entire cross-section of the ring. After eight passes of HPT, the microhardness increases by about three times as compared to the initial state from 1080 MPa to 3160 MPa. At the same time, the main increase in hardness (60%) occurs on the first four passes.

The mechanisms of microstructure evolution during deformation to various deformation degrees are clearly reflected in the distribution of

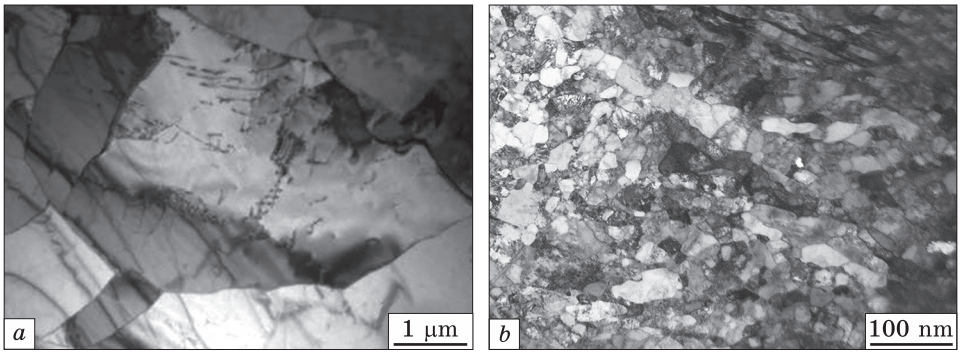

Fig. 8. Microstructure of AISI-316 steel: initial state (*a*) and after eight passes of the HPT at –196 °C (*b*) [60]

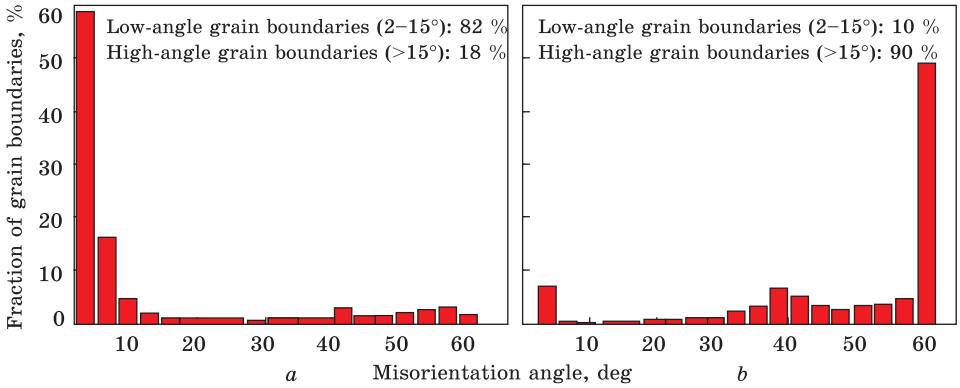

Fig. 9. Histograms of the misorientation angles after initial state (*a*) and after eight passes of the HPT at –196 °C (*b*)

grain boundaries at the disorientation angles (Fig. 9). This distribution before deformation is characterized by three distinctive peaks that correspond to angles less than 10°, angles about 45° and angles about 60°. The first peak is associated with the formation of small-angle subboundaries during plastic deformation. The second peak corresponding to the boundaries with a misorientation of ≈45° is associated with the course of the martensitic transformation by a shear mechanism. The third peak characterizes the development of deformation twinning processes [65].

The analysis of Fig. 9 showed that the misorientation of deformation subboundaries increases during deformation, *i.e.*, the proportion of small-angle subboundaries decreases with an increase of deformation degree. Deformation twinning, characteristic of small deformation degrees, when using cryogenic cooling, does not fade even on the 8th deformation cycle, as evidenced by the presence of a peak with a misorientation angle of ≈60° (Fig. 9, *b*). The share of small-angle boundaries is of

10%. The total share of large-angle boundaries is 90%, which suggests the formation of a nanocrystalline structure with a predominance of large-angle boundaries.

Cryogenic deformation is accompanied by martensitic transformation. The place of martensitic phases' origin was the intersection of shear microstrips, which are the preferred places of deformation martensite origin; their appearance contributes to the proportion growth of martensite at intermediate deformation degrees. Martensitic transformation, which took place in the most deformed areas of austenite, prevented the boundaries evolution of deformation origin in this phase and slowed down the fragmentation development. Mechanical twinning was the main mechanism for the formation of large-angle boundaries in the austenitic phase. The formation of a strongly deformed microstructure after eight deformation cycles by HPT method contributed to the course of the $\gamma \rightarrow \alpha$ shear phase transformation. Thus, using cryogenic cooling after eight deformation cycles, 93% of martensite was obtained in the structure. Such a large amount of martensite arose due to a strong difference in free energies, which led to a sharp decrease in grain size compared to stable growth. In addition, the dynamic recovery at HPT is significantly suppressed due to the sudden drop in atomic diffusion at cryogenic temperature during deformation. Due to the stimulating effect of these defects on nucleation during the phase transition, a large amount of deformation martensite begins to appear already at the 2nd deformation pass.

4. Conclusions

Deform FEM-software was used to simulate the high-pressure torsion process in a new design die for annular workpieces deformation. A special feature of the stamp design is to ensure the torsion of the deforming tool with the constant rectilinear movement of the press punch due to the composite deforming tool, which includes both displacement and rotation blocks. The results of the stress–strain state study indicate that the overwhelming proportion of deformation is compression and shear, with a distribution of approximately 85% and 15%, respectively. Compression stresses reach 4.5 GPa.

The results of the laboratory study showed that, in the process of severe plastic deformation by HPT method with cryogenic cooling, the structure of the samples is significantly crushed to nanostructured. Thus, the deformation of AISI-316 steel with an average grain size of 30 microns leads to the formation of an equiaxed homogeneous microstructure of 30–40 nm in size, consisting of 90% α-martensite with a predominance of large-angle boundaries. The formation of a nanostructured state during high-pressure torsion in a new die at cryogenic tem-

perature occurs due to the action of two mechanisms. The first mechanism is associated with the fragmentation of the initial grains due to the formation of shear deformation bands and twins of deformation origin. The second mechanism is associated with the development of the phase transformation $\gamma \rightarrow \alpha$ by the shear mechanism of the formation of deformation martensite. The tensile strength increased from 595 to 1965 MPa, the yield strength increased from 320 to 1280 MPa. The plasticity value decreases from 55% to 24% compared to the initial state, but remains at a sufficient level for use. The results of the microhardness determination correlate with the data of mechanical tests; so, after the eight passes, the microhardness increases by about 3 times from 1080 to 3160 MPa.

Acknowledgement. The research was funded by the Science Committee of the Ministry of Education and Science of the Republic of Kazakhstan (Grant No. AP08856353).

REFERENCES

1. V. Kumar, S.K. Sinha, and A.K. Agarwal, *J. Tribology*, **141**, No. 3: 031301 (2019); https://doi.org/10.1115/1.4041762
2. J. Christiansen, P. Klit, A. Volund, and J.-H. Hwang, *Int. Conf. BALTTRIB 2007 (November 21–23, 2007)* (Kaunas: 2007), p. 16.
3. T.O. Olugbade and J. Lu, *Nano Mater. Sci.*, **2**: 3 (2020); https://doi.org/10.1016/j.nanoms.2020.04.002
4. Z. Ren, R. Chiang, H. Qin, V.K. Vasudevan, G.L. Doll, Y. Dong, and C. Ye, *Wear*, **458–459**: 203398 (2020); https://doi.org/10.1016/j.wear.2020.203398
5. L. Junwei, O. Zipeng, L. Shiqiang, J. Yong, and H. Yuanzhi, *Met. Sci. Heat Treat.*, **59**: 50 (2017); https://doi.org/10.1007/s11041-017-0101-5
6. K.O. Kostyk, V.O. Kostyk, and V.D. Kovalev, *Prog. Phys. Met.*, **22**, No. 1: 78 (2021); https://doi.org/10.15407/ufm.22.01.078
7. C.C. Koch, *Nanostruct. Mater.*, **9**, Nos. 1–8: 13 (1997); https://doi.org/10.1016/S0965-9773(97)00014-7
8. I.V. Alexandrov, Y.T. Zhu, T.C. Lowe, R.K. Islamgaliev, and R.Z. Valiev, *Metall. Mater. Trans. A*, **29**: 2253 (1998); https://doi.org/10.1007/s11661-998-0103-4
9. M. Furukawa, Z. Horita, M. Nemoto, and T.G. Langdon, *Mater. Sci. Eng. A*, **324**, Nos. 1–2: 82 (2002); https://doi.org/10.1016/S0921-5093(01)01288-6
10. T.G. Langdon, *Acta Mater.*, **61**, No. 19: 7035 (2013); https://doi.org/10.1016/j.actamat.2013.08.018
11. R.Z. Valiev, *Mater. Trans.*, **55**, No. 1: 13 (2014); https://doi.org/10.2320/matertrans.MA201325
12. R.Z. Valiev, R.K. Islamgaliev, and I.V. Alexandrov, *Prog. Mater. Sci.*, **45**, No. 3: 103 (2000); https://doi.org/10.1016/S0079-6425(99)00007-9

13. S. Lezhnev, A. Naizabekov, and I. Volokitina, *J. Chem. Technol. Metallurgy*, **52**: 626 (2017).
14. A. Jäger and V. Gärtnerová, *Philos. Mag. Lett.*, **92**, No. 8: 384 (2012); https://doi.org/10.1080/09500839.2012.682740
15. E. Mostaed, A. Fabrizi, F. Bonollo, and M. Vedani, *Metallurgia Italiana*, **11–12**: 5 (2015).
16. C. Banjongprasert, A. Jak-Ra, C. Domrong, U. Patakham, W. Pongsaksawad, and T. Chairuangsri, *Arch. Metallurgy Mater.*, **60**, No. 2: 887 (2015); https://doi.org/10.1515/amm-2015-0224
17. I. Sabirov, M.T. Perez-Prado, M. Murashkin, J.M. Molina-Aldareguia, E.V. Bobruk, N.F. Yunusova, and R.Z. Valiev, *Int. J. Mater. Form.*, **3**: 411 (2010); https://doi.org/10.1007/s12289-010-0794-0
18. A.B. Naizabekov, Zh.A. Ashkeev, S.N. Lezhnev, and A.R. Toleuova, *Steel in Translation*, **35**, No. 2: 37 (2005).
19. O. Krivtsova, V. Talmazan, A. Arbuz, G. Sivyakova, *Adv. Mater. Res.*, **1030–1032**: 1337 (2014); https://doi.org/10.4028/www.scientific.net/amr.1030-1032.1337
20. R. Comaneci, L.G. Bujoreanu, C. Baciu, A.M. Predescu, and D. Savastru, *Optoelectronics and Advanced Materials — Rapid Communications*, **9**, Nos. 9–10: 1322 (2015).
21. V.A. Beloshenko, A.V. Voznyak, Y.V. Voznyak, L.A. Novokshonova, V.G. Grinyov, and V.G. Krasheninnikov, *Int. J. Polymer Sci.*, **2016**: 8564245 (2016); https://doi.org/10.1155/2016/8564245
22. L. Olejnik and A. Rosochowski, *Bull. Polish Acad. Sci. — Tech. Sci.*, **53**, No. 4: 413 (2005).
23. P.M. Keshtiban, M. Zadshakouyan, and G. Faraji, *Trans. Indian Inst. Metals*, **69**: 1793 (2016); https://doi.org/10.1007/s12666-016-0840-9
24. Y. Liu, Z.X. Kang, L.L. Zhou, J.Y. Zhang, and Y.Y. Li, *Corrosion Eng. Sci. Technol.*, **51**, No. 4: 256 (2016); https://doi.org/10.1179/1743278215Y.0000000050
25. V.A. Andreyachshenko and A.B. Naizabekov, *Metalurgija*, **55**: 353 (2016); https://doaj.org/article/67e9e72103854d469a60c23763e3461a.
26. F.J. Kalahroudi, A.R. Eivani, H.R. Jafarian, A. Amouri, and R. Gholizadeh, *Mater. Sci. Eng. A*, **667**: 349 (2016); https://doi.org/10.1016/j.msea.2016.04.087
27. J.G. Kim, M. Latypov, N. Pardis, Y.E. Beygelzimer, and H.S. Kim, *Mater. Design*, **83**: 858 (2015); http://doi.org/10.1016/j.matdes.2015.06.034
28. Sh.R. Bahadori, K. Dehghani, and S.A.A.A. Mousavi, *Mater. Lett.*, **152**: 48 (2015); https://doi.org/10.1016/j.matlet.2015.03.063
29. M.I. Latypov, M.G. Lee, Y. Beygelzimer, D. Prilepo, Y. Gusar, and H.S. Kim, *Metall. Mater. Trans. A*, **47**: 1248 (2016); https://doi.org/10.1007/s11661-015-3298-1
30. M. Hawryluk, J. Ziemba, and P. Sadowski, *Measurement and Control*, **50**, No. 3: 74 (2017); https://doi.org/10.1177/0020294017707161
31. B. Cherukuri, T.S. Nedkova, and R. Srinivasan, *Mater. Sci. Eng. A*, **410–411**: 394 (2005); https://doi.org/10.1016/j.msea.2005.08.024

32. T. Sakai, A. Belyakov, R. Kaibyshev, H. Miura, and J.J. Jonas, *Prog. Mater. Sci.*, **60**: 130 (2014);
https://doi.org/10.1016/j.pmatsci.2013.09.002
33. Y. Estrin and A. Vinogradov, *Acta Mater.*, **61**, No. 3: 782 (2013);
https://doi.org/10.1016/j.actamat.2012.10.038
34. R.Z. Valiev and I.V. Aleksandrov, *Nanostrukturnyye Materialy, Poluchennyye Intensivnoy Plasticheskoy Deformatsiey* [Nanostructural Materials Obtained by the Severe Plastic Deformation] (Moscow: LOGOS: 2000) (in Russian).
35. A.P. Zhilyaev and T.G. Langdon, *Prog. Mater. Sci.*, **53**, No. 6: 893 (2008);
https://doi.org/10.1016/j.pmatsci.2008.03.002
36. C. Xu, Z. Horita, and T.G. Langdon, *Acta Mater.*, **55**, No. 1: 203 (2007);
https://doi.org/10.1016/j.actamat.2006.07.029
37. M. Jahedi, M. Knezevic, and M.H. Paydar, *J. Mater. Eng. Perform.*, **24**: 1471 (2015);
http://doi.org/10.1007/s11665-015-1426-0
38. S. Erbel, *Met. Tech.*, **6**, No. 1: 482 (1979);
https://doi.org/10.1179/030716979803276363
39. A. Alhamidi and Z. Horita, *Mater. Sci. Eng. A*, **622**: 139 (2015);
https://doi.org/10.1016/j.msea.2014.11.009
40. W. Pachla, M. Kulczyk, M. Sus-Ryszkowska, A. Mazur, and K.J. Kurzydlowski, *J. Mater. Process. Tech.*, **205**, Nos. 1–3: 173 (2008);
https://doi.org/10.1016/j.jmatprotec.2007.11.103
41. W. Wei, S.L. Wang, K.X. Wei, I.V. Alexandrov, Q.B. Du, and J. Hu, *J. Alloys Compd.*, **678**: 506 (2016);
https://doi.org/10.1016/j.jallcom.2016.04.035
42. S.K. Panigrahi, R. Jayaganthan, V. Pancholi, and M. Gupta, *Mater. Chem. Phys.*, **122**, No. 1: 188 (2010);
https://doi.org/10.1016/j.matchemphys.2010.02.032
43. S. Ramesh Kumar, K. Gudimetla, B. Tejaswi, and B. Ravisankar, *Trans. Indian Inst. Met.*, **70**: 639 (2017);
https://doi.org/10.1007/s12666-017-1073-2
44. V.L. Niranjani, K.C.H. Kumar, and V.S. Sarma, *Mater. Sci. Eng. A*, **515**, Nos. 1–2: 169 (2009);
https://doi.org/10.1016/j.msea.2009.03.077
45. I.E. Volokitina, *J. Chem. Technol. Metall.*, **55**, No. 2: 479 (2020);
https://dl.uctm.edu/journal/node/j2020-2/29_18-214_p_479-485.pdf
46. Y.S. Li, N.R. Tao, and K. Lu, *Acta Mater.*, **56**: 230 (2008);
https://doi.org/10.1016/j.actamat.2007.09.020
47. I.E. Volokitina, S.N. Lezhnev, E.P. Orlova, and G.G. Kurapov, *Key Eng. Mater.*, **684**: 346 (2016);
https://doi.org/10.4028/www.scientific.net/KEM.684.346
48. R. Kaibyshev, D. Zhemchuzhnikova, and A. Mogucheva, *Mater. Sci. Forum*, **735**: 265 (2013);
https://doi.org/10.4028/www.scientific.net/MSF.735.265
49. S.N. Lezhnev, I.E. Volokitina, and A.V. Volokitin, *Phys. Metals Metallogr.*, **118**: 1167 (2017);
https://doi.org/10.1134/S0031918X17110072
50. P. Frint, M.F.-X. Wagner, S. Weber, S. Seipp, S. Frint, and T. Lampke, *J. Mater. Process. Tech.*, **239**: 222 (2017);
https://doi.org/10.1016/j.jmatprotec.2016.08.032

51. G.G. Kurapov, E.P. Orlova, I.E. Volokitina, and A. Turdaliev, *J. Chem. Technol. Metallurgy*, **51**: 451 (2016).
52. R.Z. Valiev, I.V. Alexandrov, Y.T. Zhu, and T.C. Lowe, *J. Mater. Res.*, **17**, No. 1: 5 (2002); https://doi.org/10.1557/JMR.2002.0002
53. M. Gzyl, A. Rosochowski, E. Yakushina, and P. Wood, *Key Eng. Mater.*, **554–557**: 876 (2013); https://doi.org/10.4028/www.scientific.net/KEM.554-557.876
54. B. Gopi, N. Naga Krishna, K. Venkateswarlu, and K. Sivaprasad, *Int. J. Mater. Met. Eng.*, **6**, No. 1: 67 (2012); https://doi.org/10.5281/zenodo.1058899
55. X.H. Chen and L. Lu, *Scr. Mater.*, **57**, No. 2: 133 (2007); https://doi.org/10.1016/j.scriptamat.2007.03.029
56. G. Purcek, O. Saray, M.I. Nagimov, A.A. Nazarov, I.M. Safarov, V.N. Danilenko, O.R. Valiakhmetov, and R.R. Mulyukov, *Philos. Mag.*, **92**, No. 6: 690 (2012); https://doi.org/10.1080/14786435.2011.634842
57. Y. Wang, M. Chen, F. Zhou, and E. Ma, *Nature*, **419**: 912 (2002); https://doi.org/10.1038/nature01133
58. A. Glezer, M. Plotnikova, S. Dobatkin, N. Perov, and A. Shalimova, *Mater. Sci. Forum*, **667–669**: 1077 (2011); https://doi.org/10.4028/www.scientific.net/MSF.667-669.1077
59. S. Malekjani, P.D. Hodgson, P. Cizek, I. Sabirov, and T.B. Hilditch, *Int. J. Fatigue*, **33**, No. 5: 700 (2011); https://doi.org/10.1016/j.ijfatigue.2010.11.025
60. A. Volokitin, A. Naizabekov, I. Volokitina, S. Lezhnev, and E. Panin, *Mater. Lett.*, **304**: 130598 (2021); https://doi.org/10.1016/j.matlet.2021.130598
61. D.S. Nadig, V. Ramakrishnan, P. Sampathkumaran, and C.S. Prashanth, *AIP Conf. Proc.*, **1435**: 133 (2012); https://doi.org/10.1063/1.4712089
62. A. Volokitin, I. Volokitina, E. Panin, A. Naizabekov, and S. Lezhnev, *Metalurgija*, **60**, Nos. 3–4: 325 (2021); https://hrcak.srce.hr/256099
63. A.V. Volokitin, A.B. Naizabekov, I.E. Volokitina, and D.N. Lavrinyuk, *XVIII Int. Cong.* '*Machines. Technologies. Materials*' *(March 10–13, 2021)* (Borovets: 2021), vol. **1**, p. 48 (in Russian).
64. R. Bidulský, J. Bidulská, F.S. Gobber, T. Kvačkaj, P. Petroušek, M. Actis-Grande, K.-P. Weiss, and D. Manfredi, *Materials*, **13**, No. 15: 3328 (2020); https://doi.org/10.3390/ma13153328
65. M. Odnobokova, A. Belyakov, and R. Kaibyshev, *Adv. Eng. Mater.*, **17**, No. 12: 1812 (2015); https://doi.org/10.1002/adem.201500100
66. A.V. Volokitin, S.N. Lezhnev, E.A. Panin, and T.D. Fedorova, *XVIII Int. Cong.* '*Machines. Technologies. Materials*' *(March 10–13, 2021)* (Borovets: 2021), vol. **1**, p. 52 (in Russian).

Received 23.02.2022;
in final version, 07.05.2022

А.В. Волокітін[1], *І.Є. Волокітіна*[2], *Є.А. Панін*[1]
[1] Карагандинський індустріальний університет,
просп. Республіки, 30, 101400 Темиртау, Казахстан
[2] Рудненський індустріальний інститут,
вул. 50 років Жовтня, 38, 111500 Рудний, Казахстан

ТЕРМОМЕХАНІЧНЕ ОБРОБЛЕННЯ ПОРШНЕВИХ КІЛЕЦЬ ІЗ НЕІРЖАВІЙНОЇ КРИЦІ

Досліджується вплив термомеханічного оброблення, — інтенсивної пластичної деформації методом кручення під високим тиском і кріогенного охолодження, — на зміну мікроструктури та механічних властивостей поршневих кілець з неіржавійної криці AISI-316. Деформування кільцевих заготовок здійснюється в інструменті нової конструкції, ключовою особливістю якого є система подвійної спіралі. У першій частині експерименту проводиться оцінювальне моделювання процесу кручення під високим тиском у новій конструкції матриці. Для оцінювання можливости перебігу процесу виконується варіювання основних технологічних параметрів процесу задля визначення найбільш оптимальних умов. Вибираються такі параметри як температура нагрівання заготовки, вертикальна швидкість руху верхнього бойка та коефіцієнт тертя на контакті заготовки з інструментом. Також вивчається напружено-деформований стан кільцевої заготівки під час деформування. На другому етапі дослідження проводиться лабораторний експеримент з деформування кільцевих заготовок. Вивчається еволюція мікроструктури та механічні властивості деформованих заготовок після 8 циклів деформування методом кручення під високим тиском за кріогенної температури. Всі металографічні дослідження виконуються із залученням сучасних методів просвітлювальної електронної мікроскопії й аналізу картин дифракції зворотньо відбитих електронів. В результаті деформування одержується нанокристалічна структура розміром у 30–40 мкм з наявністю великої кількости великокутових меж і високим комплексом механічних властивостей. Межа міцности підвищується від 595 МПа до 1965 МПа, а межа плинности — від 320 до 1280 МПа. Значення пластичности понижується порівняно з вихідним станом від 55% до 24%, проте залишається на достатньому для використань рівні.

Ключові слова: інтенсивна пластична деформація, поршневі кільця, неіржавійна криця, мікроструктура, механічні властивості, кріогенне охолодження.